Geosfera Indonesia
p-ISSN 2598-9723, e-ISSN 2614-8528
available online at : https://jurnal.unej.ac.id/index.php/GEOSI
Vol. 9 No. 1, April 2024, 1-15

https://doi.org/10.19184/geosi.v9i1.38154

Research Article

Heavy Rain Episodes Identified by L-band InSAR and Limitations of Split-Spectrum Method in Indonesia

Naufal Setiawan[1]*, Masato Furuya[2]
[1] Department of Geomatic Engineering, Faculty of Mineral Technology, Universitas Pembangunan Nasional "Veteran" Yogyakarta, Indonesia
[2]Department of Earth and Planetary Sciences, Faculty of Science, Hokkaido University, Sapporo, Japan
*Corresponding author, email : naufal.setiawan@upnyk.ac.id

ARTICLE INFO

Received :
20 February 2023

Revised :
10 March 2024

Accepted :
29 March 2024

Published :
7 April 2024

ABSTRACT

Located in a tropical area with abundant precipitation, Indonesia is highly prone to heavy rain hazards, in particular landslides and floods. Thus, rainfall observation is vital. Nonetheless, the topography, the fund availability, as well as the archipelagic state of Indonesia may raise difficulties for in-situ observation, such as rain gauge and weather radar. Currently, the advance of radiometer satellites, such as the Global Precipitation Mission delivers rain estimation and has proven to show good association with in-situ observation on a monthly basis, not daily over the Indonesia area. Therefore, it is vital to have additional measurement methods. For the first time, we apply L-band Interferometric Synthetic Aperture Radar (InSAR) to observe heavy rain in Indonesia. From our three study cases, we successfully identified localized anomalies due to the dense water vapor during heavy rain in the InSAR images. The localized anomalies vary from 10.9 cm in West Java, 7.8 cm in East Kalimantan, and 7.7 cm in West Kalimantan. Furthermore, we utilize the split-spectrum method for our InSAR result; the high-water vapor occurrence in the troposphere associated with heavy rain should be identified in the non-dispersive term. Nevertheless, due to long temporal separation and thinner bandwidth, the split-spectrum method results display unsatisfactory results. We conclude that, while InSAR has the ability to identify heavy rain, having SSM to distinguish between non-dispersive and dispersive phases is not currently practical in Indonesia.

Keywords : Indonesia heavy rain; InSAR; split-spectrum method

INTRODUCTION

Indonesia is a tropical country and has only two seasons throughout the year, dry and wet seasons. Generally, the El Nino Southern Oscillation (ENSO) affects Indonesia's climate. The dry season commonly covers from May to September, while the wet season covers from December until February (Lee, 2015). Throughout the year, Indonesia has an enormous amount of precipitation and considered as one of the atmospheric heat sources of the Earth's climate system (Supari et al., 2012).

Heavy rain is one of the roots of numerous hazards in Indonesia; for instance, landslides and floods. Subsequently, it may have serious impact on economy and society (Halimatussadiah et al., 2018). Therefore, direct rainfall monitoring using rain gauge station is important. However, heavy rainfall may occur locally where rain gauge station is not always available. This condition simply causes heavy rainfall events to be un-observed by the rain gauge station. Thus, continuous spatial monitoring using weather radar is a better option in Indonesia. However, due to several

limitations, such as topographic challenge, wide area, and fund availability, some areas are not covered by weather radar (Permana et al., 2019).

Alternatively, we can use Global Satellite Mapping of Precipitation (GSMaP) for rainfall estimation. GSMaP is a product of the Global Precipitation Mission (GPM) project which uses radiometer satellites, such as Tropical Rainfall Measuring Mission (TRMM) and geostationary infrared satellite. The GSMaP aims to develop a precipitation rate retrieval algorithm and produce global rainfall maps from satellite data (Okamoto et al., 2005). One of the GSMaP product is GSMaP Moving Vector with Kalman filter (GSMaP_MVK) which utilizes a Kalman filter model to improve the rainfall rate propagated from two consecutive data (Ushio et al., 2009). However, the GSMaP data do not always show a good agreement with rain gauge data on monthly average and low to medium correlation in the daily average rainfall (Setiyoko et al., 2019). Therefore, additional rainfall observation in Indonesia will be valuable.

Synthetic Aperture Radar (SAR) is an active imaging radar and unique in terms of its capability to observe the earth independent from day light and cloud coverage. The Single Look Complex Image (SLC) of SAR consists of amplitude and phase value with high spatial resolution, with 5m X 5m or better. The amplitude of SLC in a single SAR acquisition is usable after reducing the speckle noise (multi-looking). Although the phase image in a single SAR acquisition is impractical because it is impossible to interpret the physical meaning (Furuya, 2011). Exploiting the range delay between two SAR images, Interferometric Synthetic Aperture Radar (InSAR) has been proven to measure deformation related not only to natural disasters (earthquake (Massonnet et al., 1993), volcano eruption (Biggs et al., 2009), glacier retreat (Yasuda & Furuya, 2015) but also monitoring man-made objects (mining deformation monitoring) (Yang et al., 2020). Additionally, in the absence of surface deformation, but substantial atmosphere phenomena occur, we can detect such occurrences utilizing InSAR. For instance, Sporadic-E in the ionosphere layer (Maeda et al., 2016) as well as heavy downpours due to large water vapor entities in the troposphere (Hanssen, 1998). Furthermore, given the raindrop properties that are able to scatter the electromagnetic wave, Setiawan & Furuya (2021) proved that by utilizing the modification of the Split-Spectrum Method (Gomba et al., 2016), the detection of dispersive phase due to dense raindrops during heavy rain is achievable. Nevertheless, their test site is limited only to the Japan region.

There are two objectives in this study. Both objectives, as far as we know, have been never reported by previous researchers in Indonesia areas. First, to test the capability of InSAR to detect heavy rain signals in Indonesia by following the concept given by Hanssen (1998). Second, is to test the applicability of SSM following the original concept as Gomba et al. (2016) in Indonesia heavy rain. Our study areas are limited to three areas, West Kalimantan, East Kalimantan, and West Java (Figure 1). The primary reason is to obtain heavy rain events (more than 50 mm/ hour) that adjacent to Advanced Land Observation Satellite/ Phased Array type L-band Synthetic Aperture Radar (ALOS/ PALSAR) and ALOS-2/ PALSAR-2 are not always available.

METHODS

GSMaP for Searching Possible Heavy Rain

This study used research and development (R&D) method or often referred to as a type of development research. We search for possible heavy rain cases in Indonesia, particularly in Java and Kalimantan (Figure 1) from GSMaP_MVK data (Ushio et al., 2009; Setiyoko et al., 2019). After that, we check the availability of ALOS/ PALSAR for Fine Beam Single (FBS) polarization mode spanning from 2007 until 2011; the chirp bandwidth in the FBS mode is 32MHz. We also look for possible heavy rain cases during ALOS-2/PALSAR-2 for Strip Map-3 (SM-3) mode from 2014 until 2018; the chirp bandwidth in the SM-3 mode is 34.9MHz. There is no surface deformation related to the earthquake in the possible heavy rain cases according to the United States Geological Survey (USGS) earthquake catalog.

Furthermore, to minimize the ionospheric disturbance, we select heavy rain at local night time coincide with ascending observation of ALOS/PALSAR and ALOS-2/PALSAR-2 (Figure 2b, 3b, 4a). To provide further investigation during InSAR processing, we also search for other ALOS/PALSAR and ALOS-2/PALSAR-2 data with no or very little precipitation (Figures 2a, 2c, 3a,

3c, 4b, 4c). These allow us to create heavy rain-as well as fair-weather interferogram pair. We identified one possible heavy rain case in Java (West Java, Figure 3b) on July 23, 2018 1700UTC and two possible heavy rain cases in Kalimantan. One in East Kalimantan (Figure 4a), on January 24, 2015 1600UTC, and West Kalimantan (Figure 5a), on February 14, 2007 1500UTC. Table 1 describes the ALOS/PALSAR and ALOS-2/PALSAR-2 data utilized in this study.

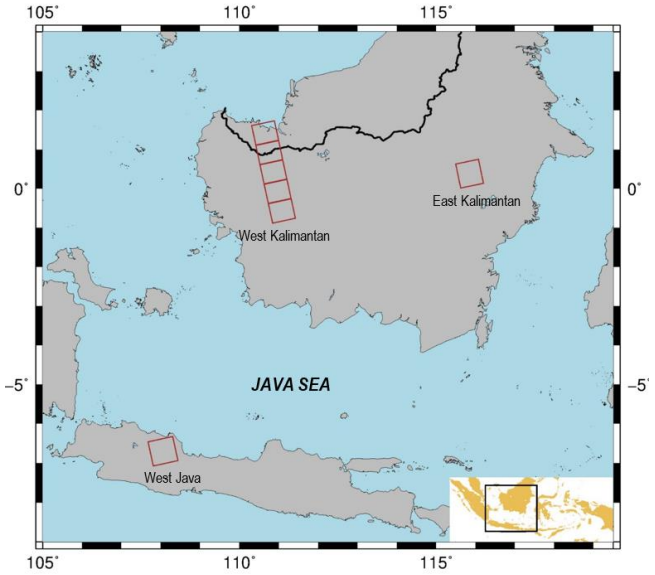

Figure 1. Study areas: Red rectangle indicates ALOS-2/PALSAR-2 or ALOS/ PALSAR frame.

Table 1. Details of ALOS/PALSAR and ALOS-2/PALSAR-2 data for Indonesia heavy rain cases

Scene ID	Path Number	Frame Number	Obs Centre Time (UTC)	Precipitation	Area
ALOS2199397050-180131	134	7050	2018/01/31 17:06:00	no	West Java
ALOS2215957050-180523	134	7050	2018/05/23 17:06:00	yes	
ALOS2224237050-180718	134	7050	2018/07/18 17:06:00	no	
ALOS2015607190-140906	129	7190	2014/09/06 16:30:18	no	East Kalimantan
ALOS2036307190-150124	129	7190	2015/01/24 16:30:17	yes	
ALOS2090127190-160123	129	7190	2016/01/23 16:30:14	no	
ALPSRP056387170	427	7170	2007/02/14 15:23:31	yes	West Kalimantan
ALPSRP056387180	427	7180	2007/02/14 15:23:39		
ALPSRP056387190	427	7190	2007/02/14 15:23:48		

Scene ID	Path Number	Frame Number	Obs Centre Time (UTC)	Precipitation	Area
ALPSRP056390000	473	0	2007/02/14 15:23:56		
ALPSRP056390010	473	10	2007/02/14 15:24:04		
ALPSRP110067170	427	7170	2008/02/17 15:21:52		
ALPSRP110067180	427	7180	2008/02/17 15:22:05		
ALPSRP110067190	427	7190	2008/02/17 15:22:13	no	
ALPSRP110070000	473	0	2008/02/17 15:22:21		
ALPSRP110070010	473	10	2008/02/17 15:22:29		
ALPSRP157037170	427	7170	2009/01/04 15:23:06		
ALPSRP157037180	427	7180	2009/01/04 15:23:10		
ALPSRP157037190	427	7190	2009/01/04 15:23:19	no	
ALPSRP157040000	473	0	2009/01/04 15:23:31		
ALPSRP157040010	473	10	2009/01/04 15:23:35		

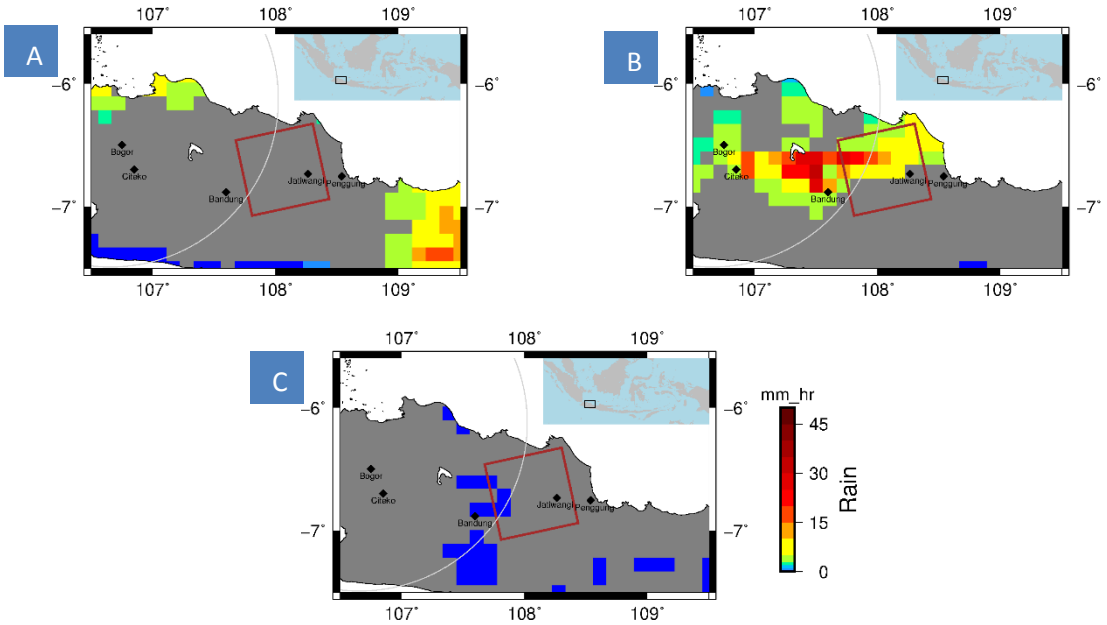

Figure 2. GSMaP MVK on West Java (a) 20180131_1700UTC, (b) 20180523_1700UTC, and (c)20180718_1700UTC, where we express the observed year (YYYY), month (MM), day (DD) with YYYYMMDD. GSMaP estimate precipitation around 40 mm/hr in 20180523. Red rectangle indicates ALOS-2/PALSAR-2 frame. The black diamond mark with city name indicate rain gauge station location.

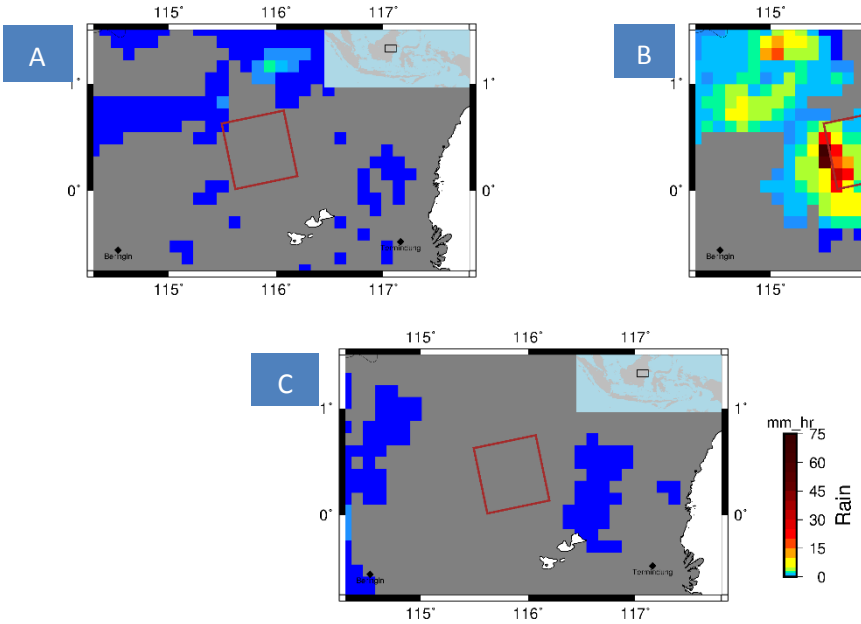

Figure 3. GSMaP MVK on East Kalimantan, (a) 20140906_1600UTC, (b) 20150124_1600UTC, , and (c) 20160123_1600UTC. GSMaP estimate precipitation around 65 mm/hr in 20150124. Red rectangle indicates ALOS-2/PALSAR-2 frame. The black diamond mark with city name indicate rain gauge station location.

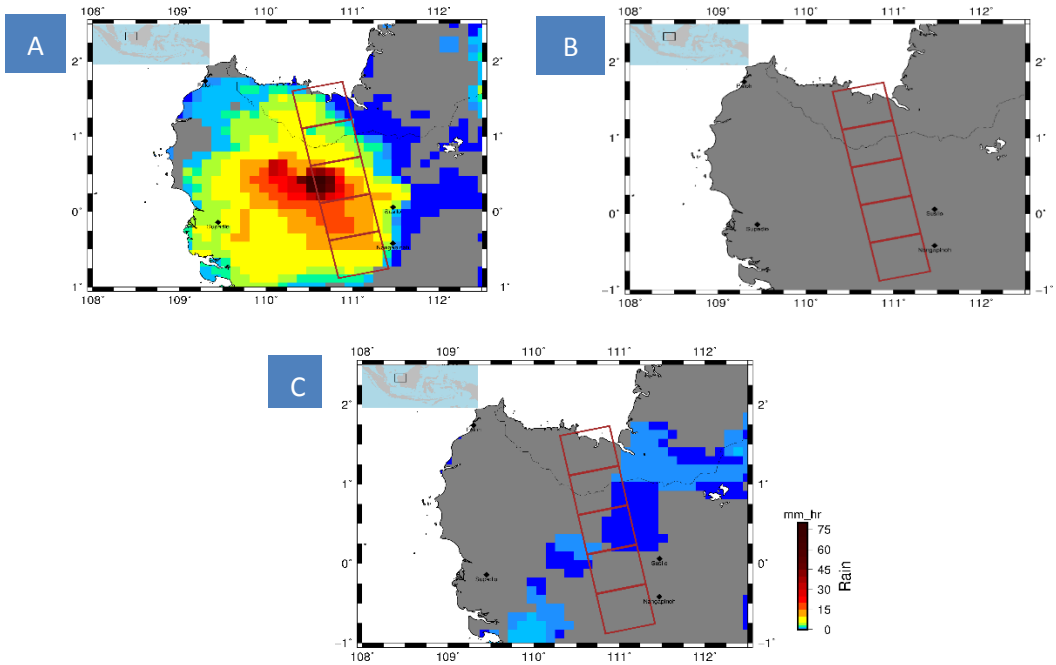

Figure 4. GSMaP MVK on West Kalimantan (a) 20070214_1500UTC, (b) GSMaP on 20080217_1500UTC, and (c) 20090104_1500UTC (right). GSMaP estimate precipitation around 50 mm/hr in 20150124. Red rectangle indicates ALOS/PALSAR frames. The black diamond mark with city name indicate rain gauge station location.

InSAR Processing Method

We used GAMMA processing software licensed to Space Geodesy Laboratory, Hokkaido University, for both InSAR and SSM processing. During InSAR processing, only the West Kalimantan images are concatenated between consecutive frames. We apply total multi-looking (in range and azimuth) of 30 and 90 for West Kalimantan, 27 and 36 for West Java, 36 and 48 for

East Kalimantan, which results in the spatial resolutions of ~140m for West Kalimantan, ~115m for West Java, and ~154m for East Kalimantan in range and ~289m for West Kalimantan, ~137m for West Java, and ~157m for East Kalimantan in azimuth, respectively. Then, we remove topographic fringe by using ALOS World 3D-30m (AW3D30) DEM data (~30 m x 30 m resolution). The unwrapping procedure utilize the minimum-cost flow algorithm (Costantini, 1998). To preserve our interpretation, we do not apply long-wavelength phase trends correction.

SSM Processing Method

The effect of the ionosphere layer on InSAR may complicate the interpretation of the result if not treated correctly. Thus, several methods could mitigate ionospheric influence particularly in the L-band InSAR, for example; range phase group delay (Meyer et al., 2006), multiple aperture interferometry and its along-track integration (Jung et al., 2013), or split-spectrum method (Brcic et al., 2011; Rosen et al., 2010; Gomba et al., 2016)).

A microwave traversing through the ionosphere experience two different effects, the first effect is the phase advance of the microwave carrier due to the free electrons (Belcher, 2008).

$$\emptyset_{ionosphere} = \frac{4\pi K}{cf}\,\mathrm{TEC} \tag{1}$$

In the above equation, TEC is the abbreviation of total electron content, K = 40.28 m^3/s^2, c is the speed of light, and f is the carrier frequency. The second effect of the microwave pass through the ionosphere is the Faraday rotation. Since the second effect is minimum, it is neglected in the split-spectrum method (Gomba et al., 2016). The split-spectrum method (SSM) takes advantage of the dispersive nature of the ionosphere, as clearly stated in equation 3, to separate from the non-dispersive contribution (Gomba et al., 2016).

$$\Delta\emptyset = \frac{4\pi f_0}{c}\left(\Delta\emptyset_{deformation} + \Delta\emptyset_{troposphere}\right) + \frac{4\pi}{c f_0}\Delta\emptyset_{ionosphere} \tag{2}$$

In practice, the range split-spectrum method divides the original bandwidth of the SAR observation into smaller bandwidth with its new high and low frequency. At this point, interferograms of high and low sub-band can be created using the standard InSAR processing, following Gomba et al., (2016) and Furuya et al., (2017);

$$\begin{aligned}\Delta\emptyset_H &= \Delta\emptyset_{non-dispersive}\frac{f_H}{f_0} + \Delta\emptyset_{dispersive}\frac{f_0}{f_H}\\ \Delta\emptyset_L &= \Delta\emptyset_{non-dispersive}\frac{f_L}{f_0} + \Delta\emptyset_{dispersive}\frac{f_0}{f_L}\end{aligned} \tag{3}$$

Then, one could estimate the non-dispersive phase ($\Delta\emptyset_{deformation}$ and $\Delta\emptyset_{troposphere}$) and dispersive phase ($\Delta\emptyset_{ionosphere}$) (Gomba et al., 2016; Furuya et al., 2017).

$$\begin{aligned}\Delta\emptyset_{non-dispersive} &= \frac{f_0}{(f_H^2 - f_L^2)}\left(\Delta\emptyset_H f_H - \Delta\emptyset_L f_L\right)\\ \Delta\emptyset_{dispersive} &= \frac{f_H f_L}{f_0\,(f_H^2 - f_L^2)}\left(\Delta\emptyset_L f_H - \Delta\emptyset_H f_L\right)\end{aligned} \tag{4}$$

If during InSAR observation, no deformation took places, we can isolate the water vapor contribution in the troposphere during heavy rain using the above equation. Furthermore, using a modified SSM, a recent study reported a possible detection of the dispersive signal of heavy rain (Setiawan & Furuya, 2021).

Two new interferograms with small bandwidth and new center frequency are created from original bandwidth using the SSM with each new sub-bands a third of the original bandwidth. The SSM processing strategy follows (Furuya et al., 2017). We use a total multi-looking with a factor 63 and 84 in range and azimuth for West Java and 72 and 96 in range and azimuth for East Kalimantan cases. Meanwhile, we apply a total multi-looking with a factor of 48 and 144 in range

and azimuth for West Kalimantan case. This step was done to accommodate coarser range resolution derived from the new thinner bandwidth.

RESULTS

The processing result of InSAR is summarized in Table 2 for three different regions. Figure 5 shows the InSAR processing result in West Java. There are some localized anomalies 10.9 cm moving toward the satellite line of sight in the heavy rain pair (Figure 5a). Meanwhile, in the no precipitation pair (Figure 5b), there is no similar localized anomaly identified.

Table 2. Summary of InSAR processing results

Region	Heavy rain InSAR pairs	Tropospheric anomaly occurrence	Maximum Quantities	Fair-weather InSAR pairs	Tropospheric anomaly occurrence
West Java	20180523_20180718	Yes	10.9 cm	20180131_20180718	No
East Kalimantan	20150124_20160123	Yes	7.7 cm	20140906_20160123	No (but ionospheric noise detected)
West Kalimantan	20070214_20080217	Yes	7.8 cm	20080217_20090104	No

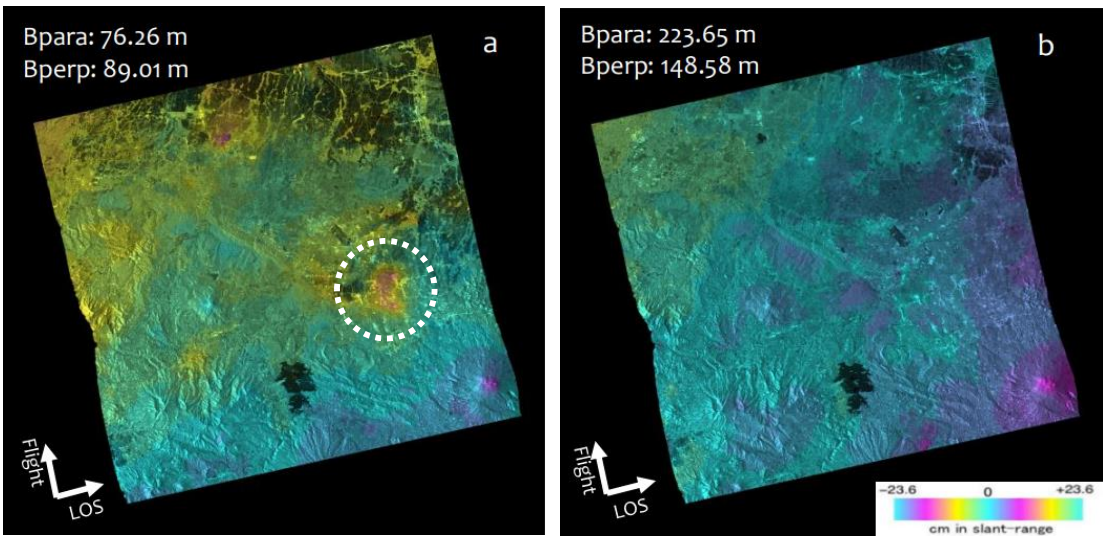

Figure 5. InSAR processing result West Java; (a) 20180523_20180718, (b) 20180131_20180718. The InSAR area is indicated by red rectangle in Figure 1. White-dashed circle showed the anomaly in InSAR result

Figure 6 shows the InSAR processing result in East Kalimantan. Some localized anomalies reach 7.7 cm approaching toward the satellite line of sight in the heavy rain pair (Figure 6a). Meanwhile, in the fair-weather pair (Figure 6b), there is no similar localized anomaly identified, whereas there is a long-wavelength trend in the fair-weather pair (Figure 6b), probably due to the ionosphere contribution. Furthermore, low coherence due to long temporal separation cause gap in the interferogram.

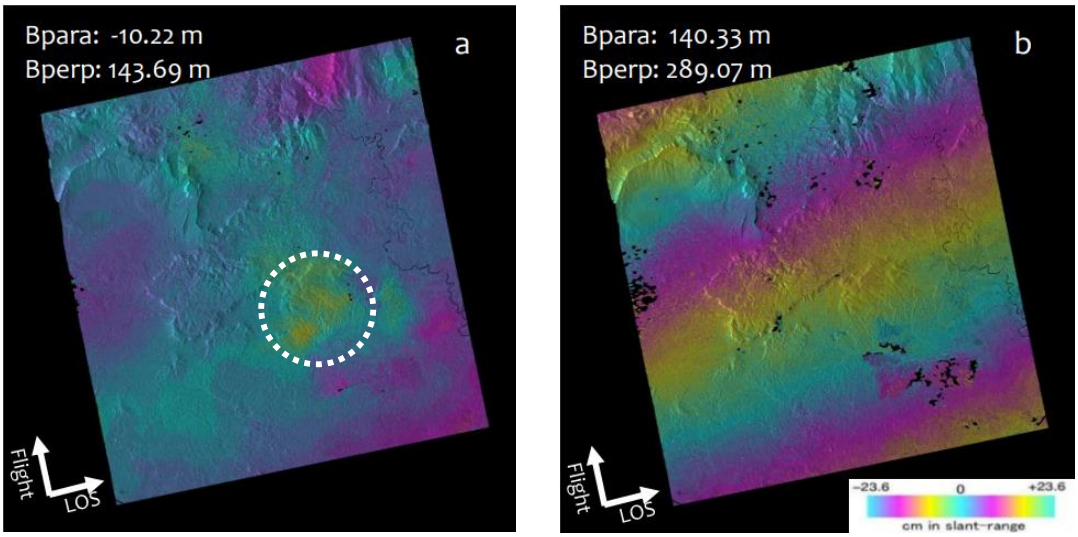

Figure 6. InSAR processing result East Kalimantan; (a) 20150124_20160123, (b) 20140906_20160123. The InSAR area is indicated by red rectangle in Figure 2. White-dashed circle showed the anomaly in InSAR result.

Figure 7 shows the InSAR processing result in West Kalimantan. Some localized anomalies reach 7.8 cm approaching the satellite line of sight in the heavy rain pair (Figure 7a). Meanwhile, in the no precipitation pair (Figure 7b), there is no similar localized anomaly identified.

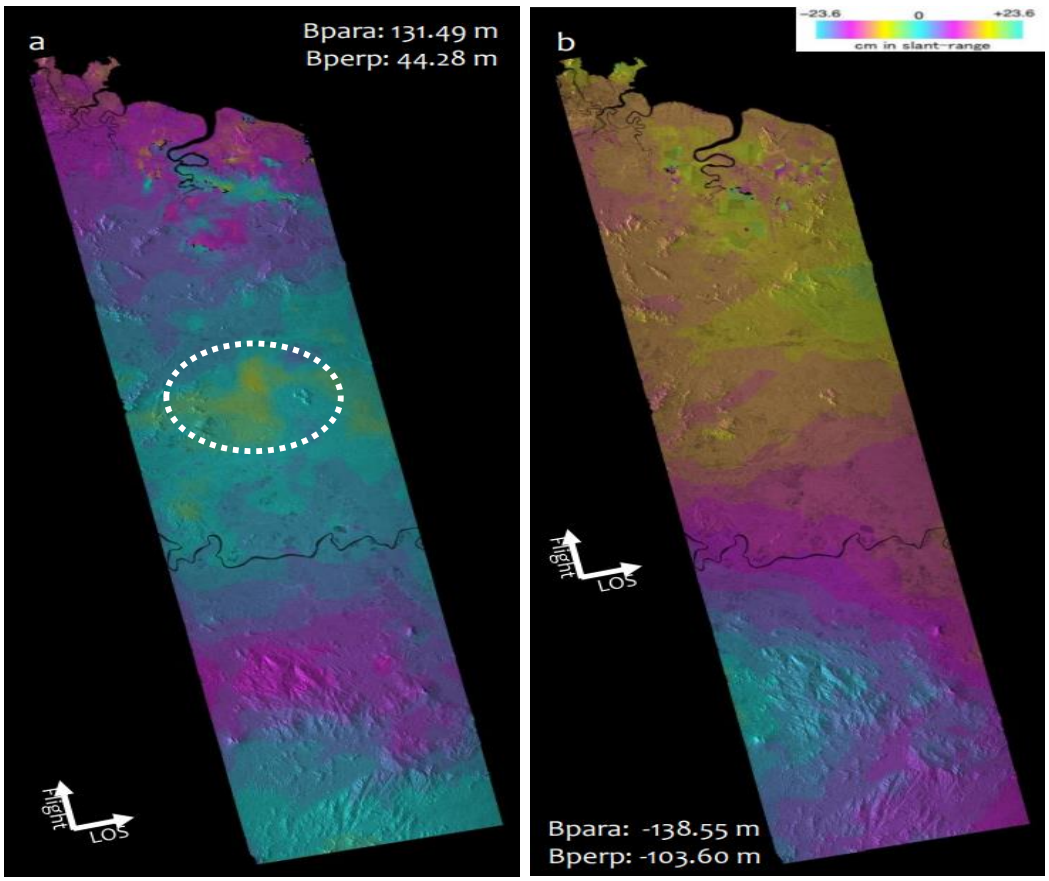

Figure 7. InSAR processing result West Kalimantan; (a) 20070214_20080217, (b) 20080217_20090104. The InSAR area is indicated by red rectangle in Figure 3. White-dashed circle showed the anomaly in InSAR result.

SSM Processing Result

We estimate non-dispersive and dispersive phase using the equation 4. Despite the retrieval of non-dispersive and dispersive phase are not satisfactory, we identify some of the pattern in the non-dispersive phase related to the occurrence of water vapor in West Java and only slight pattern in West Kalimantan (Figures 8a, 10a). The East Kalimantan non-dispersive and dispersive phases are not interpretable (Figures 9a, b).

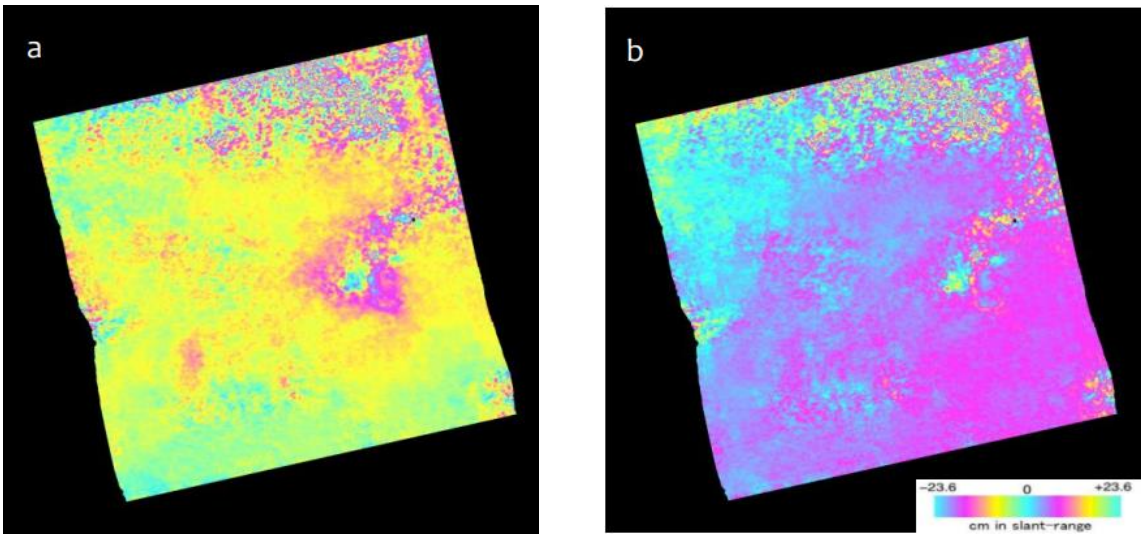

Figure 8. The (a) non-dispersive phase and (b) the dispersive phase of West Java heavy rain (20180523_20180718).

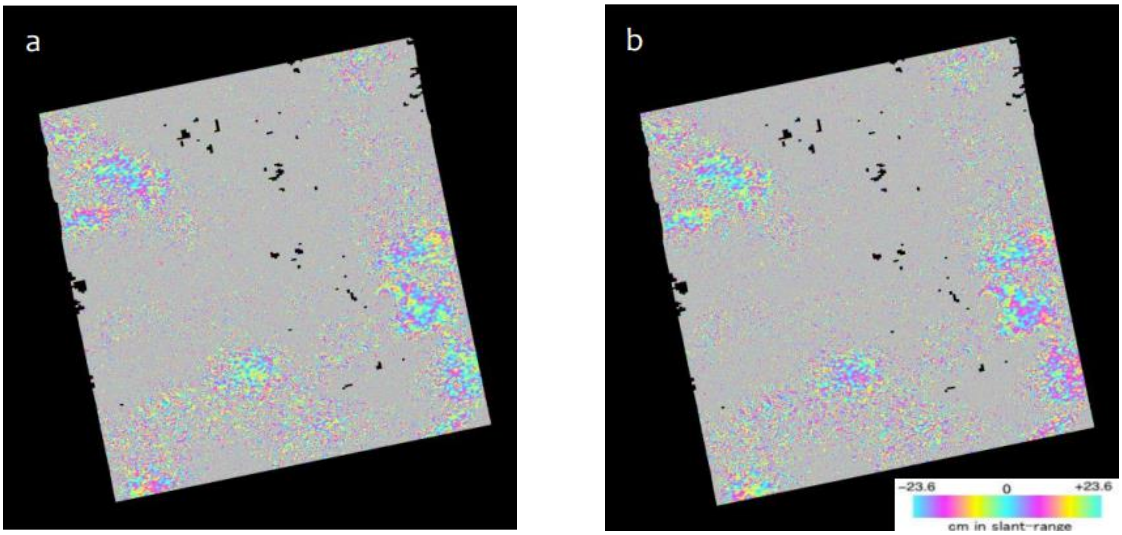

Figure 9. The (a) non-dispersive phase and (b) the dispersive phase of East Kalimantan heavy rain (20150124_20160123).

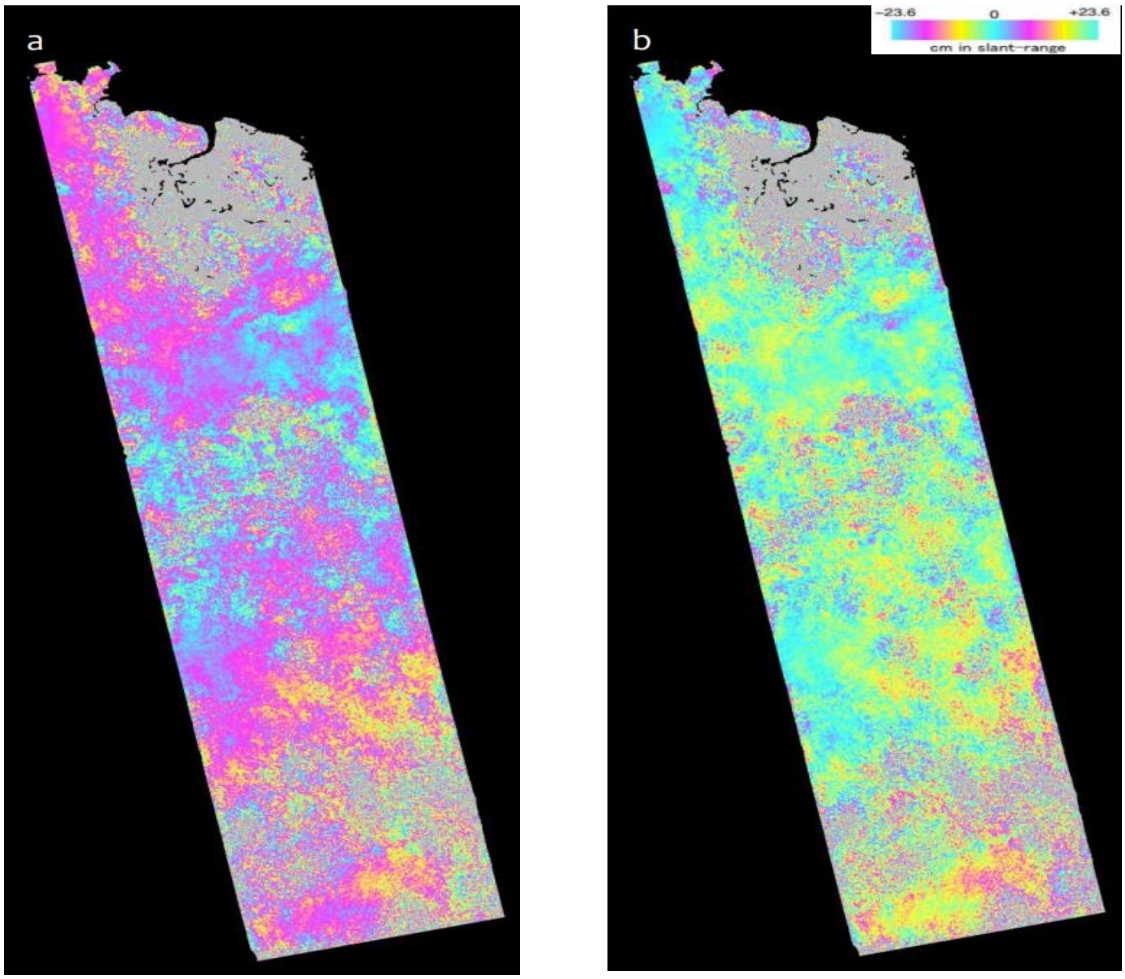

Figure 10. The (a) non-dispersive phase and (b) the dispersive phase of West Kalimantan heavy rain (20070214_20080217)

DISCUSSION

Interpreting the Dense Water Vapor Occurrence in the Troposphere from InSAR Images

InSAR exploits the range difference between the two-phase in the same path and frame of SAR acquisition. This is denoted as two-way travel time;

$$\Delta\emptyset = \frac{4\pi}{\lambda}(r_1 - r_2) \quad (5)$$

where λ is the wavelength, r_1 is the range in the first SAR acquisition, and r_2 is the range in the second SAR acquisitions. The phase difference contains;

$$\Delta\emptyset = \Delta\emptyset_{orbit} + \Delta\emptyset_{topo} + \Delta\emptyset_{def} + \Delta\emptyset_{atm} \quad (6)$$

The orbital fringe ($\Delta\emptyset_{orbit}$) appears because the SAR satellite cannot observe from the same position and can be removed using precise satellite orbit. $\Delta\emptyset_{topo}$ is related to the topographic fringe. $\Delta\emptyset_{orbit}$ and $\Delta\emptyset_{topo}$ can be removed by using the satellite orbital data and the external Digital Elevation Model (DEM), respectively. The $\Delta\emptyset_{def}$is the deformation fringe that occurred due to surface movement (such as earthquake or magma movement beneath the volcano). The $\Delta\emptyset_{atm}$ is the atmospheric fringe appearing due to the change of refractive index of the atmospheric layer. These fringes resulted in the phase delay; $\Delta\emptyset_{atm}$ can be further separated into two components based on the dispersive ionosphere and the non-dispersive troposphere (Hanssen, 2002). Therefore, if only $\Delta\emptyset_{atm}$ of the troposphere identifiable, InSAR can be used to observe tropospheric water vapor distributions associated with heavy rain (Kinoshita et al.,

2013). It is vital to note the tropospheric phase value is not absolute, but relative since the observation time is different (between master t_1 and t_2); thus, atmospheric condition also varies.

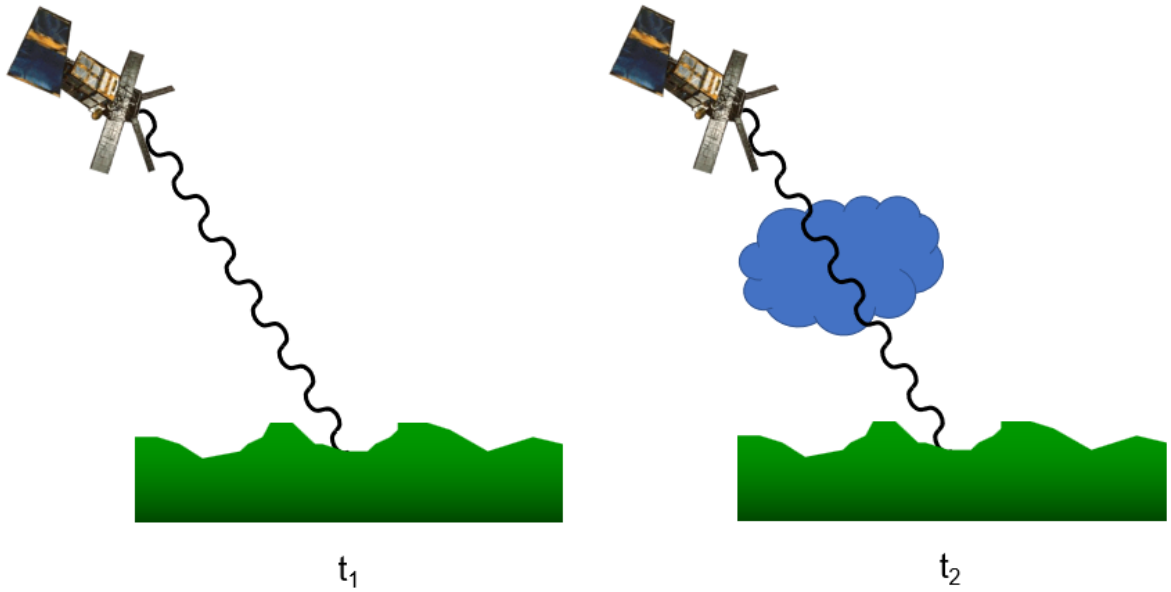

Figure 11. A simple illustration of dense water vapor detection using the InSAR method during two consecutive (t_1 and t_2) SAR observations.

All the InSAR component phases in our research area are already eliminated, except the $\Delta\emptyset_{atm}$. Therefore, the localized anomalies in InSAR images are related to water vapor during heavy rain (Hanssen, 1998; Mateus et al., 2012; Kinoshita et al., 2013; Mateus et al., 2017). The localized anomalies are successfully recognized in three case studies of InSAR heavy rain images in Indonesia. As a prove that the anomaly is related to heavy rain, InSAR fair-weather pairs do not display similar localized anomaly.

Ionospheric Noise in East Kalimantan InSAR Image and Comparison with Global Ionospheric Model derived from GNSS

The InSAR result of the fair-weather pair in East Kalimantan (20140906_20160123) showed a long wavelength trend identical to ionospheric noise (Figure 6b). Meanwhile, the heavy rain pair in East Kalimantan (20150124_20160123) does not exhibit a similar pattern (Figure 6a). To prove our explanation of ionospheric noise in the InSAR image, we plot the Total Electron Content (TEC) acquired from independent measurement by using another geodetic instrument, the Global Navigation Satellite System (GNSS). GNSS utilize dual-frequency L-band measurement to model the ionospheric delay due to the TEC (Jakowski et al., 2006; Jin et al., 2022). Using these data, it is confirmed that the long-wave phase trend is due to higher TEC on 20140906 (Figure 12). The Total Electron Content Unit (TECU) in 20140906 reached a maximum of 45, while in 20150124 peaked at 20 TECU and only 10 TECU in 20160123. In terms of InSAR satellites, TEC detection in the ionosphere affects the L-band ALOS/ PALSAR and ALOS-2/ PALSAR-2 (Gomba et al., 2016; Brcic et al., 2011; Meyer et al., 2006; Maeda et al., 2016 ; Furuya et al., 2017) more than other InSAR satellite, for instance, C-band Sentinel-1 (Liang et al., 2019).

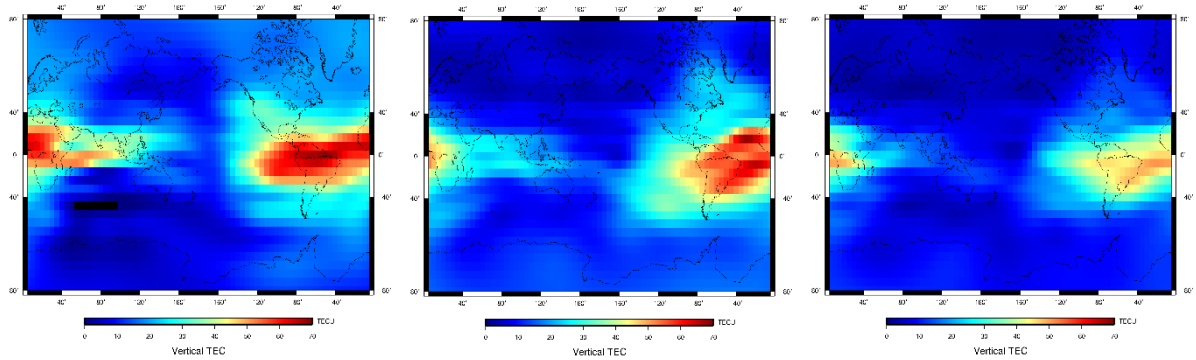

(a) (b) (c)

Figure 12. The Global Ionosphere Model (http://ftp.aiub.unibe.ch/CODE/#) at 16.33 UTC, (a) 20140906, (b) 20150124, and (c) 20160123.

SSM Limitation in Indonesia Heavy Rain Cases

We attempt to validate using SSM following (Gomba et al., 2016), since there is no large deformation due to earthquakes occuring, the non-dispersive phase will detect the vast water vapor occurrence due to heavy rain. The result varies from poor (East Kalimantan) to identifiable with some noises (West Java and West Kalimantan). Compared with previous research (Gomba et al., 2016; Furuya et al., 2017), the possible reason for this unsatisfactory result is due to the long-temporal separation between the data observation (ALOS/PALSAR). Moreover, compared to the SM-1 mode of ALOS-2/ PALSAR-2 (Setiawan & Furuya, 2021) the acquisition mode in the Indonesia area has a much smaller bandwidth (SM-3 of ALOS-2/PALSAR-2).

It is evident for the SSM to get a satisfactory result; the wider the bandwidth in the frequency modulation, the better the range resolution. Nevertheless, the opportunity to observe heavy rain using L-band InSAR and SSM validation in Indonesia will increase as the NISAR (NASA-ISRO SAR Mission) satellite will launch into orbit in the upcoming year. Furthermore, as the opportunity increases, we may regularly utilize InSAR data to increase weather forecast accuracy in Indonesia (Mateus et al., 2017).

CONCLUSION

For the first time, we apply InSAR in Indonesia heavy rain cases using L-band ALOS/ PALSAR and ALOS-2/ PALSAR-2 data. InSAR successfully identified anomalies due to the abundant water vapor in the troposphere during heavy rain (West Java 10.9 cm, East Kalimantan 7.8 cm, West Kalimantan 7.7 cm). Nonetheless, the SSM results is not satisfactory, due to the long temporal separation and the smaller bandwidth of the acquisition mode in Indonesia area. Our research concludes, that L-band InSAR shows potential in heavy rain detection over Indonesia areas, but to have SSM successfully separate between non-dispersive and dispersive is not yet feasible in Indonesia.

ACKNOWLEDGMENTS

The ALOS-2/PALSAR-2 level 1.1 data in this study are shared among PIXEL (PALSAR Interferometry Consortium to Study our Evolving Land Surface) under a cooperative research contract with the Earthquake Research Institute, University of Tokyo. The ownership of ALOS-2/PALSAR-2 data belongs to the JAXA (Japan Aerospace Exploration Agency). The Global Rainfall Map (GSMaP) by JAXA Global Rainfall Watch was produced and distributed by the Earth Observation Research Center, JAXA. The Global Ionosphere Model is accessed from the http://ftp.aiub.unibe.ch/CODE/#).

DECLARATIONS

Conflict of Interest

The authors declared that they had no known competing interests.

Ethical Approval

On behalf of all authors, the corresponding author states that the paper satisfies Ethical Standards conditions, no human participants, or animals are involved in the research.

Informed Consent

On behalf of all authors, the corresponding author states that no human participants are involved in the research and, therefore, informed consent is not required by them.

DATA AVAILABILITY

Data used to support the findings of this study are available from the corresponding author upon request.

REFERENCES

Belcher, D. P. (2008). Theoretical limits on SAR imposed by the ionosphere. *IET Radar Sonar and Navigation*, *2*(4), 274–283. https://doi.org/10.1049/iet-rsn

Biggs, J., Anthony, E. Y., & Ebinger, C. J. (2009). Multiple inflation and deflation events at Kenyan volcanoes, East African Rift. *Geology*, *37*(11), 979–982. https://doi.org/10.1130/G30133A.1

Brcic, R., Parizzi, A., Eineder, M., Bamler, R., & Meyer, F. (2011). Ionospheric effects in SAR interferometry: An analysis and comparison of methods for their estimation. *International Geoscience and Remote Sensing Symposium (IGARSS)*, 1497–1500. https://doi.org/10.1109/IGARSS.2011.6049351

Costantini, M. (1998). A novel phase unwrapping method based on network programming. *IEEE Transactions on geoscience and remote sensing*, 36(3), 813-821.

Furuya, M., Suzuki, T., Maeda, J., & Heki, K. (2017). Midlatitude sporadic-E episodes viewed by L-band split-spectrum InSAR. *Earth, Planets and Space*, *69*(1). https://doi.org/10.1186/s40623-017-0764-6

Furuya, M. (2011). *Sar Interferometry*. 1–24. Encyclopedia of Solid Earth Geophysics. Springer. https://doi.org/10.1007/978-90-481-8702-7

Gomba, G., Parizzi, A., De Zan, F., Eineder, M., & Bamler, R. (2016). Toward operational compensation of ionospheric effects in SAR interferograms: The split-spectrum method. *IEEE Transactions on Geoscience and Remote Sensing*, *54*(3), 1446–1461. https://doi.org/10.1109/TGRS.2015.2481079

Halimatussadiah, A., Resosudarmo, B. P., & Widyawati, D. (2017). Social capital to induce a contribution to environmental collective action: results from a laboratory experiment in Indonesia. *International Journal of Environment and Sustainable Development, 16*(4), 397-414. https://doi.org/10.1504/IJESD.2017.087262

Hanssen, R. (1998). *Atmospheric heterogeneities in ERS tandem SAR interferometry* (Issue 98). Retrieved from http://doris.tudelft.nl/Literature/hanssen98i.html.

Hanssen, R. F. (2002). *Radar Interferometry, Data Interpretation and Error Analysis*. Springer Science & Business Media.

Jakowski, N., Heise, S., Stankov, S. M., & Tsybulya, K. (2006). Remote sensing of the ionosphere by space-based GNSS observations. *Advances in Space Research*, *38*(11), 2337–2343. https://doi.org/10.1016/j.asr.2005.07.015

Jin, S., Wang, Q., & Dardanelli, G. (2022). A review on multi-GNSS for earth observation and emerging applications*. Remote Sensing, 14*(16), https://doi.org/10.3390/rs14163930

Jung, H. S., Lee, D. T., Lu, Z., & Won, J. S. (2013). Ionospheric correction of SAR interferograms by multiple-aperture interferometry. *IEEE Transactions on Geoscience and Remote Sensing*, *51*(5), 3191–3199. https://doi.org/10.1109/TGRS.2012.2218660

Kinoshita, Y., Shimada, M., & Furuya, M. (2013). InSAR observation and numerical modeling of the water vapor signal during a heavy rain: A case study of the 2008 Seino event, central Japan. *Geophysical Research Letters*, *40*(17), 4740–4744. https://doi.org/10.1002/grl.50891

Lee, H. (2015). General Rainfall Patterns in Indonesia and the Potential Impacts of Local Seas on Rainfall Intensity. *Water*, *7*(12), 1751–1768. https://doi.org/10.3390/w7041751

Liang, C., Agram, P., Simons, M., & Fielding, E. J. (2019). Ionospheric correction of InSAR time series analysis of C-band sentinel-1 TOPS data. *IEEE Transactions on Geoscience and Remote Sensing*, *57*(9), 6755–6773. https://doi.org/10.1109/TGRS.2019.2908494

Maeda, J., Suzuki, T., Furuya, M., & Heki, K. (2016). Imaging the midlatitude sporadic e plasma patches with a coordinated observation of spaceborne InSAR and GPS total electron content. *Geophysical Research Letters*, *43*(4), 1419–1425. https://doi.org/10.1002/2015GL067585

Massonnet, D., Rossi, M., Carmona, C., Adragna, F., Peltzer, G., Feigl, K., & Rabaute, T. (1993). The displacement field of the Landers earthquake mapped by radar interferometry. *nature*, 364(6433), 138-142.

Mateus, P., Catalao, J., & Nico, G. (2017). Sentinel-1 Interferometric SAR mapping of precipitable water vapor over a country-spanning area. *IEEE Transactions on Geoscience and Remote Sensing*, *55*(5), 2993–2999. https://doi.org/10.1109/TGRS.2017.2658342

Mateus, P., Nico, G., Tom, R., & Catal, J. (2012). *on the Mitigation of Atmospheric Phase Delay Artefacts in Interferometric Sar Time Series*. *Retrieved from https://www.esa.int/*

Meyer, F., Bamler, R., Jakowski, N., & Fritz, T. (2006). The potential of low-frequency SAR systems for mapping ionospheric TEC distributions. *IEEE Geoscience and Remote Sensing Letters*, *3*(4), 560–564. https://doi.org/10.1109/LGRS.2006.882148

Okamoto, K., Ushio, T., Iguchi, T., Takahashi, N., & Iwanami, K. (2005). The Global Satellite Mapping of Precipitation (GSMaP) project. *International Geoscience and Remote Sensing Symposium (IGARSS)*, *5*(3), 3414–3416. https://doi.org/10.1109/IGARSS.2005.1526575

Permana, D. S., Hutapea, T. D., Praja, A. S., Paski, J. A. I., Makmur, E. E. S., Haryoko, U., Umam, I. H., Saepudin, M., & Adriyanto, R. (2019). The Indonesia In-House Radar Integration System (InaRAISE) of Indonesian Agency for Meteorology Climatology and Geophysics (BMKG): Development, Constraint, and Progress. *IOP Conference Series: Earth and Environmental Science, 303*(1). https://doi.org/10.1088/1755-1315/303/1/012051

Rosen, P. A., Hensley, S., & Chen, C. (2010). Measurement and mitigation of the ionosphere in L-band Interferometric SAR data. *IEEE National Radar Conference - Proceedings*, 1459–1463. https://doi.org/10.1109/RADAR.2010.5494385

Setiawan, N., & Furuya, M. (2021). Tropospheric dispersive phase anomalies during heavy rain detected by L-band InSAR and their interpretation. *Earth, Planets and Space*, *73*(1). https://doi.org/10.1186/s40623-021-01470-9

Setiyoko, A., Osawa, T., & Nuarsa, W. (2019). Evaluation of GSMaP Precipitation Estimates Over Indonesia. *International Journal of Environment and Geosciences*, *3*(1), 43. https://doi.org/10.24843/ijeg.2019.v03.i01.p04

Supari S., Sudibyakto S., Ettema, J., & Aldrian, E. (2012). Spatiotemporal characteristics of extreme rainfall events Over Java Island, Indonesia. *Indonesian Journal of Geography*, *44*(1), 62-86.

Ushio, T., Sasashige, K., Kubota, T., Shige, S., Okamoto, K., Aonashi, K., Inoue, T., Takahashi, N., Iguchi, T., Kachi, M., Oki, R., Morimoto, T., & Kawasaki, Z. I. (2009). A kalman filter approach to the global satellite mapping of precipitation (GSMaP) from combined passive microwave and infrared radiometric data. *Journal of the Meteorological Society of Japan*, *87 A*, 137–151. https://doi.org/10.2151/jmsj.87A.137

Yang, Z., Li, Z., Zhu, J., Wang, Y., & Wu, L. (2020). Use of SAR/InSAR in mining deformation monitoring, parameter inversion, and forward predictions: A review. *IEEE Geoscience and Remote Sensing Magazine, 8*(1), 71-90. https://doi.org/10.1109/MGRS.2019.2954824

Yasuda, T., & Furuya, M. (2015). Dynamics of surge-type glaciers in West Kunlun Shan, Northwestern Tibet. *Journal of Geophysical Research: Earth Surface*, *120*(11), 2393–2405. https://doi.org/10.1002/2015JF003511